Neurobiology of Disease 45 (2012) 583–590

Contents lists available at SciVerse ScienceDirect

Neurobiology of Disease

journal homepage: www.elsevier.com/locate/ynbdi

Decoupling neuronal oscillations during subthalamic nucleus stimulation in the parkinsonian primate

A. Moran, E. Stein, H. Tischler, I. Bar-Gad *

Gonda Multidisciplinary Brain Research Center, Bar Ilan University, Ramat Gan 52900, Israel

ARTICLE INFO

Article history:
Received 10 July 2011
Revised 25 September 2011
Accepted 29 September 2011
Available online 7 October 2011

Keywords:
Parkinson's disease
Deep brain stimulation (DBS)
Oscillations
Subthalamic nucleus (STN)
Non-human primate
1-methyl-4-phenyl-1,2,3,6-tetrahydropyridine (MPTP)

ABSTRACT

Subthalamic nucleus (STN) stimulation is a popular treatment for Parkinson's disease; however, its effect on neuronal activity is unclear. We performed simultaneous multi-electrode recordings in the STN and its targets, the globus pallidus internus (GPi) and externus (GPe) in the parkinsonian non-human primate during high frequency STN macro-stimulation. Our results indicate that in the parkinsonian state the abnormal neuronal oscillatory activity in the 10–15 Hz range is coherent within and between nuclei. We further show that STN macro-stimulation results in a reduction of oscillatory activity in the globus pallidus. In addition, a functional decoupling of the STN from its pallidal targets is evidenced by the reduced STN–GPi coherence, that effectively removes the STN synchronous oscillatory drive of basal ganglia output. This decoupling results in reduced coherence between neurons within the GPi which resume an independent neuronal activity pattern. This decorrelation of the basal ganglia output may result in a reduction of the fluctuations of the basal ganglia inhibitory control over thalamic neurons which may potentially contribute to the beneficial effects of deep brain high-frequency stimulation.

Introduction

Parkinson's disease (PD) is a neurodegenerative disorder whose motor symptoms derive primarily from the loss of midbrain dopaminergic neurons. The reduced dopaminergic innervation to the striatum results in abnormal neuronal activity throughout the cortico-basal ganglia (BG) loop. Lesions in the subthalamic nucleus (STN) were shown to reduce PD symptoms in the non-human primate model of the disease (Bergman et al., 1990). Subsequent application of STN high frequency stimulation (HFS) improved parkinsonian symptoms (Benazzouz et al., 1993; Limousin et al., 1995) leading to the popularization of deep brain stimulation (DBS).

Early perception of the pathophysiology underlying the clinical symptoms of PD and their subsequent amelioration using HFS focused on firing rate changes (Albin et al., 1989; DeLong, 1990). This perception ascertained that during PD the mean activity of the output nucleus of the BG, the globus pallidus internus (GPi), is excessive, leading to reduced cortical activity resulting in hypokinetic symptoms. This elevated GPi activity was attributed, in part, to increased excitation from the STN. Following this line of reasoning, it was predicted that lesions of the STN would ameliorate parkinsonian symptoms by reducing BG output, thereby leading to increased cortical activity. STN-HFS was indeed found to inhibit local STN neuronal activity (Filali et al., 2004; Meissner et al., 2005; Welter et al., 2004). However, studies of the direct target of the STN innervation, the GPi, did not confirm the expected reduction in firing rate during stimulation, demonstrating instead either no change or an increase in the mean firing rate (Hashimoto et al., 2003; Moran et al., 2011).

Recent studies of the neurophysiological changes during PD have shifted to changes in firing patterns. Neuronal activity in the normal BG is characterized by "random" patterns in both the temporal (non-oscillatory Poissonian spiking) and spatial (non-coherent and uncorrelated activity) domains (Bergman et al., 1994; Heimer et al., 2002; Nini et al., 1995; Raz et al., 2000). In the parkinsonian state, BG neuronal activity becomes oscillatory and coherent (Bergman et al., 1994; Brown et al., 2001; Nini et al., 1995). These spectral changes appear in two different frequency bands: a low tremor-frequency band (5–7 Hz) and a higher frequency band (>10 Hz) associated with PD hypokinetic symptoms (Moran et al., 2008; Zaidel et al., 2009). These synchronized oscillations are reduced following dopamine replacement treatment (Brown et al., 2001; Heimer et al., 2002; Levy et al., 2002). STN-HFS reduces spiking oscillations in the STN (Meissner et al., 2005) and local field potential (LFP) oscillations in the STN and GPi in conjunction with a reduction in PD symptoms (Brown et al., 2004; Kuhn et al., 2008; Pogosyan et al., 2010).

Abbreviations: BG, basal ganglia; BUA, background unit activity; DBS, deep brain stimulation; GPe, globus pallidus externus; GPi, globus pallidus internus; HFS, high frequency stimulation; LFP, local field potentials; MPTP, 1-methyl-4-phenyl-1,2,3,6-tetrahydropyridine; PD, Parkinson's disease; STN, subthalamic nucleus.

* Corresponding author at: Gonda Brain Research Center, Bar-Ilan University, Ramat Gan 52900, Israel. Fax: +972 3 5352184.
E-mail address: bargadi@mail.biu.ac.il (I. Bar-Gad).

Available online on ScienceDirect (www.sciencedirect.com).

0969-9961/$ – see front matter © 2011 Elsevier Inc. All rights reserved.
doi:10.1016/j.nbd.2011.09.016

These findings heighten the need to unravel the STN-HFS induced changes in the transmission of neural spiking oscillations from the stimulation site to the GPi and the ensuing changes it induces in the properties of BG output. We pursued this goal by performing simultaneous multi-electrode recordings in the STN, GPe and GPi before and during STN-HFS in the parkinsonian primate. These recordings enable the assessment of STN-HFS effects on activity propagation along the cortico-BG loop and serve to study the potential mechanism of PD symptom amelioration.

Methods

Animals

Two Macaca fascicularis male monkeys (N—4 kg; P—4.5 kg) were used in this study. The monkeys' water and food consumption and weight were followed daily and their health was monitored by a veterinarian. All procedures were in accordance with the National Institutes of Health Guide for the Care and Use of Laboratory Animals and Bar-Ilan University guidelines for the use and care of laboratory animals in research and were approved and supervised by the Institutional Animal Care and Use Committee.

Surgery and induction of parkinsonism

The monkeys underwent a surgical procedure to attach a 27 mm square Cilux recording chamber (Alpha-Omega Engineering, Nazareth, Israel) to the skull allowing access to the basal ganglia. The chamber was tilted 40° (monkey N) or 35° (monkey P) in the sagittal plane, with its center targeted at stereotaxic coordinates A13–L8–H13 of monkey N's left hemisphere, and A12–L6–H12 of monkey P's right hemisphere (Szabo and Cowan, 1984). The surgical procedure was performed under aseptic conditions and isoflurane and N_2O general anesthesia. Parkinsonism was induced by five intramuscular injections of 0.4 mg/kg 1-methyl-4-phenyl-1,2,3,6-tetrahydropyridine (MPTP)-HCl under intramuscular Ketamine-HCl (10 mg/kg) anesthesia over a period of 4 days (2 injections during the first day), after which the monkeys developed severe parkinsonism. This common MPTP protocol leads to a rapid and massive bilateral reduction in the dopaminergic neuronal population. This protocol and other protocols which focus on either unilateral milder symptoms, or slowly progressing symptoms mimicking the disease progression are reviewed elsewhere (Fox and Brotchie, 2010). The clinical manifestation included all the main parkinsonian symptoms except for rest tremor, which is typically not exhibited by this species. Additionally, both monkeys had dystonia, primarily in the lower limbs. The monkeys' parkinsonian state was assessed daily and was severe and stable throughout the recording period (mean ± SD: monkey N: 46.6 ± 2.7, monkey P: 44.0 ± 2.7, Schneider scale of 0 (asymptomatic) to 53 (maximal symptoms) (Schneider et al., 2003)). Recordings in both monkeys were resumed 5 days after the last MPTP injection.

Recording and stimulation

The monkeys were seated in a primate chair and their head was fixed during the recording sessions. The vigilance of the monkeys was monitored online using 2–4 video camera streams to avoid periods of drowsiness or closed eyes (Adler et al., 2010). Eleven glass or Narylene coated tungsten recording microelectrodes (impedance 0.2–0.7 MΩ at 1 kHz, We-Sense, Nazareth, Israel) and one concentric electrode composed of a Narylene coated tungsten recording microelectrode (impedance 0.5 MΩ at 1 kHz) surrounded by a Narylene coated 28 gauge canula (impedance 2 KΩ at 1 kHz) serving as a stimulation macroelectrode were advanced separately (EPS 4.10, Alpha–Omega Engineering) into the STN and GP. The two electrode towers allowed different trajectories to the GP (8 microelectrodes) and STN (3 microelectrodes and one concentric electrode) with 10° between the towers. The distinction between the pallidal segments was determined online based on characteristics of neuronal activity, and the existence of border cells and white matter fibers between the two segments. All the GPe neurons used in this study were high-frequency pausers. STN trajectories were performed through the internal capsule, until reaching the STN which was identified by large and highly oscillating background activity, and isolated single units with a firing rate of 20–30 spikes/s. The stimulation position within the STN relied both on recording STN activity with the concentric inner recording microelectrode and by leveling the concentric outer macro-contact to other recording electrodes. All stimulation locations were at least 0.5 mm ventral to the STN dorsal border. The electrodes' signals were continuously sampled at 40 kHz (Alphamap 10.10, Alpha–Omega Engineering), amplified (*1000) and wide bandpass filtered (2–8000 Hz four-pole Butterworth filter) (MCP-Plus 4.10, Alpha–Omega Engineering). High frequency monophasic cathodal stimulation voltage stabilized pulses (2 V, 60 μs, leading to a peak current of ~1 mA) were delivered via the macro-electrode using an optically isolated stimulator (STG-2008, Multichannel Systems, Reutlingen, Germany). Higher voltage amplitudes (4 V) induced pyramidal effects (muscle contractions), mimicking similar effects found in human STN DBS surgeries. The interval between consecutive pulses was 8 ms, leading to a stimulation frequency of 125 Hz. Recording sessions consisted of 60 s of baseline activity followed by ~125 s (15,600 pulses) of stimulation. Previous studies using the same configuration have demonstrated that the neuronal response to the stimulation reaches a steady state within less than 30 s (Moran et al., 2011).

Histology

Following completion of the experiment, the animals were anesthetized using ketamine-HCl (10 mg/kg) and stereotactic marking micro-lesions (DC cathodal current, 60 μA for 30 s) were made. The animals were then deeply anesthetized using sodium pentobarbital (50 mg/kg) and transcardially perfused with 1 l of physiological saline, followed by 1 l of 4% paraformaldehyde. The whole brain was removed and buffered in graded sucrose solution 10–30% over seven days. The brain was then frozen at −25 °C and cut in the coronal plane using a cryostat (Leica Microsystems). Each section was digitized using a 10 MPixel digital camera and sections of interest were mounted onto glass slides and Nissl stained. The locations of all the stimulation and recording sites were determined based on their relation to the micro-lesion locations (Moran et al., 2011).

Data analysis

The digitized continuous signal was pre-processed to remove the stimulation artifacts using our stimulus artifact removal graphical environment (SARGE) (Erez et al., 2010) (Fig. 1). Specifically, we utilized a moving average calculation using a running window whose size was adjusted to maximize signal quality after artifact removal (typically 30–40 consecutive pulses) or in cases of unstable artifacts, the local polynomial fit algorithm. The signal was then offline sorted (OFS-2.8.4, Plexon, Dallas, TX) to generate one or more spike trains. The spike train quality was verified by observing less than 0.1% short (<1 ms) inter-spike-intervals and stability was verified by checking that the spike shape was not significantly altered throughout the session. All further data analysis was performed using custom written MATLAB code (Mathworks, Natick, MA).

The spike timestamps found using the offline sorting procedure were used to reconstruct the background unit activity (BUA). In this procedure, the traces in the segments from 0.5 before to 2.5 ms after each spike timestamp (including unsorted spikes) in the high-pass (250 Hz) filtered trace were replaced by a spike-free consecutive signal from a random location within the same recorded trace (Moran and

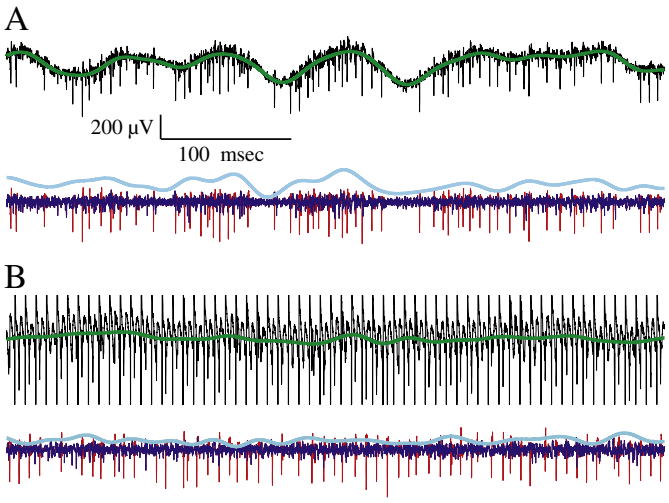

Fig. 1. Neuronal activity before and during stimulation. (A) Example trace of a recording from an electrode located within the GPi prior to stimulation. The wide band filtered signal (top, black) is filtered to generate the different signals: the low pass filtered LFP (top, green), the high passed neuronal activity (bottom, red), the spike removed activity BUA (bottom, dark blue) and the low pass filtered BUA envelope (bottom, light blue, double scale). (B) Recording of the same electrode during stimulation. The top graph depicts the raw trace while the bottom trace shows the same trace after stimulus artifact suppression and filtering. Color coding as shown in (A).

Bar-Gad, 2010; Moran et al., 2008). Next, the BUA signal was rectified and low-pass (500 Hz) filtered. Only the last 60 s of the stimulation period were used for analyzing the stimulation effects to avoid the early dynamic changes (Erez et al., 2009; Moran et al., 2011).

Power spectral density (PSD) was calculated using Welch's method utilizing 1000 bin windows on the 1000 sample/s down-sampled signals resulting in a 1 Hz spectral resolution. The PSD was scaled by the mean power in the 5–40 Hz range. Single neurons were defined as having significant oscillations if they had a peak in the PSD which displayed significant increased power ($p<0.01$, 2.4 STD difference) compared to the power in the 20–40 Hz band and a higher power than the 7–9 Hz band. The distribution of the PSD did not follow a normal distribution and thus comparison of different states (before vs. during stimulation) was done using the non-parametric Wilcoxon paired signed rank test which examines the state pairs for each neuron. These two assessment methods, the magnitude of the power reduction (assessed by the fraction of the PSD) and the non-parametric significance of the change (assessed by the Wilcoxon test), are not necessarily identical and rather provide two measures of describing the change in the system.

Coherence was calculated with the same parameters used for the PSD. The difference between coherences before vs. during stimulation was calculated in three steps: (1) Subtraction of the baseline coherence (mean coherence 60–90 Hz) from both coherence functions. (2) The *coherence peak value (Cp)* was defined as the maximal value in the 10–15 Hz frequency band. (3) Coherence reduction was calculated by:

$$C_{diff} = 100 \cdot \frac{C_p(during) - C_p(before)}{C_p(before)}$$

Coherence between spike trains (single units — SUs) and BUAs was calculated only for SU–BUA pairs from different electrodes to avoid residual correlation effects. The coherograms were calculated using a running window of 4 s with 3 s overlap. The population coherogram was the mean of all pair-wise coherograms smoothed with a 2D Gaussian filter of size 5×5 and $\sigma=0.7$. Coherence values are highly dependent on the number of windows used. Thus, we have normalized the coherogram values (based on low window count) to the range of values of the overall coherence (based on high window count) by subtracting the difference between the mean coherences in the 20–30 Hz range from all coherogram values. This normalization process did not change the pattern of the coherogram across the frequency/time domain but only its baseline value.

Results

HFS was applied to the STN of two parkinsonian primates using stimulation parameters comparable to those used in human DBS (voltage stabilized, 2 V, 60 μs cathodal pulses at a rate of 125 pulses/s). The activity of 49 GPi, 70 GPe and 36 STN neurons was recorded before and during stimulation. All the neurons were sorted offline and passed the criteria for well separated single units (SUs). The same dataset was previously used to analyze static and dynamic properties of firing modulation to the stimulation (Moran et al., 2011). Prior to the stimulation onset some of the neurons in all three structures displayed significant oscillatory activity within the 10–15 Hz range which was typically centered around 12–13 Hz (GPi 22/49 45%, GPe 18/70 26% and STN 13/36 36%). Spectral analysis of the activity of GPe and GPi neurons recorded in the normal primate revealed that none (0/53) had significant oscillatory activity. The mean power in the 10–15 Hz band of the oscillatory neurons displayed a mean decrease during STN-HFS in the GPe and GPi but not in the STN (Figs. 2A–B). Analysis of paired single neuron oscillations before and during the stimulation revealed a significant stimulation-dependent decrease in the peak power within the 10–15 Hz band for both the GPi and GPe ($p<0.01$, Wilcoxon paired signed rank test) but not in the STN ($p>0.05$). The power distribution did not follow a normal distribution and thus the significance of the change between states (before vs. during stimulation) was done in a paired manner using a non-parametric test.

The spectral content of background unit activity (BUA), which represents the spiking activity of a local neuronal population (Moran and Bar-Gad, 2010), was examined following the removal of stimulation artifacts and any identified single units (Fig. 2C). Overall, 40 recordings from the GPi, 55 from the GPe and 27 from the STN were analyzed. In line with the single unit recordings, the spectral power displayed the same oscillatory phenomenon; moreover, the pre-stimulation oscillations and their decrease during stimulation were larger. The mean PSD of BUAs for each location demonstrated significant peaks between 10 and 15 Hz prior to stimulation (Fig. 2D). In the GPi the high oscillatory content was reduced significantly across the population by the stimulation ($p<0.001$ Wilcoxon paired signed rank test), and more moderately in the STN ($p<0.01$, Wilcoxon paired signed rank test, although the mean power changed in only a smaller manner). In the GPe, as can be expected from the small fraction of significantly oscillating single units, no significant reduction in the BUA was found ($p>0.05$).

The oscillatory interaction between the neuronal activity in the STN and its targets was assessed using the coherence between different neuronal signals. The mean coherence between all simultaneously recorded pairs of STN-BUA and GPi-BUA prior to the stimulation was elevated in the 10–15 Hz band with a maximal value at 12–13 Hz (Fig. 3A). STN-HFS led to the reduction of the coherence peak value to baseline level (92% decrease in the peak coherence during stimulation relative to the baseline coherence). The drop in the coherence between STN–GPi BUA encompassed the vast majority of STN–GPi pairs (34/38, 89%) which displayed decreased values during the stimulation ($p<0.001$, Wilcoxon paired signed rank test) (Fig. 3B). The mean STN–GPi BUA pair coherogram (time dependent coherence) indicated that the drop in coherence was immediate (<1 s) following the initiation of the stimulation period and did not change afterwards during the entire stimulation period (Fig. 3C). Coherence between the different signals (LFP, BUA and SU) from the STN and GPi revealed that the

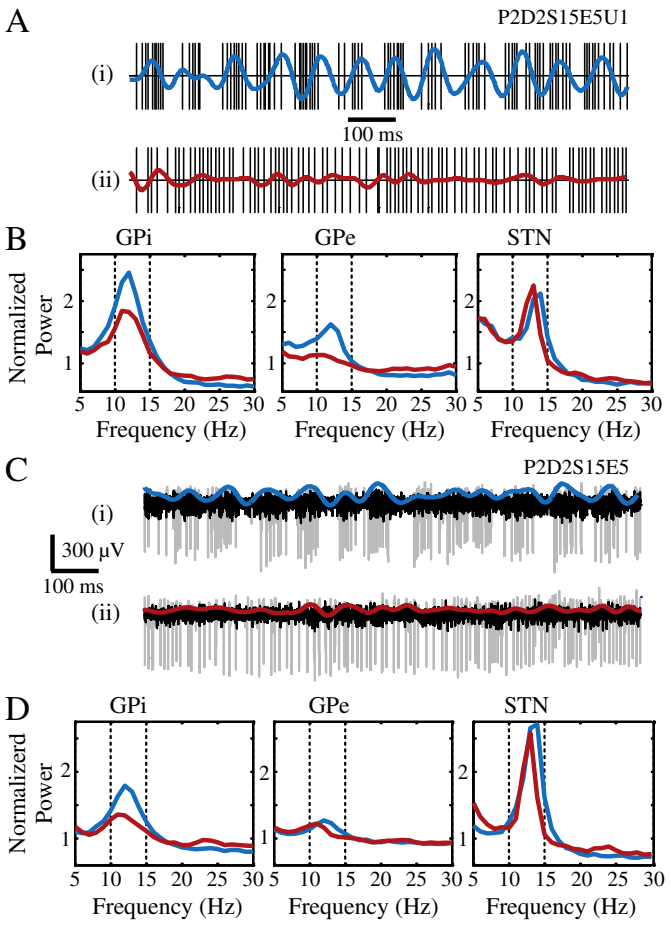

Fig. 2. Oscillatory activity. (A) Example of a GPi SU (black bars) overlaid with its band pass (5–20 Hz) filtered signal, (i) before (blue) and (ii) during (red) stimulation. (B) Mean PSD of the SU oscillatory sub-population before (blue) and during (red) stimulation. (C) Example of a recorded GPi signal (gray) and its corresponding BUA (black) overlaid with the band passed (5–20 Hz) filtered BUA envelope signal, (i) before (blue) and (ii) during (red) stimulation. (D) Mean PSD of the whole BUA population before (blue) and during (red) stimulation.

same decoupling of the two nuclei occurred across all the coherence measures (Fig. 3D). The decrease in measures of the nuclei output signals (SU and BUA) was approximately the same but the rank significance of the SUs was smaller as most of the SU decrease was due to a smaller fraction of the population. Even the LFP, which represents a more global signal biased toward the input to the nuclei, presented a significant decrease in its coherence. The decrease in coupling occurred between the STN and its other target nucleus, the GPe (Fig. 3E). However, the weaker oscillations of the parkinsonian GPe resulted in reduced coherence with the STN prior to the stimulation and consequently a smaller decrease in the coherence during stimulation. The small fraction of oscillating GPe SUs also resulted in non-significant rank changes in the SU coherence despite the large reduction in the coherence magnitude.

The oscillatory activity in the 10–15 Hz range was coherent between the two segments of the GP (GPe and GPi) prior to the stimulation and was reduced by the stimulation (49% reduction in the population GPe–GPi BUA coherence, $p<0.01$, Wilcoxon paired signed rank test) (Fig. 4A). This reduction was much smaller than the one observed between the STN and either of the GP segments. The change in the coherence over time (Fig. 4B) and the coherence measure between the different signals (LFP, BUA and SU) from the GPe and GPi revealed that the same smaller decoupling of the two nuclei occurred across all the coherence measures (Fig. 4C).

The oscillatory activity in the 10–15 Hz range within the GPi was coherent across recording electrodes prior to the stimulation. The coherence peak value of BUA signals from different electrodes was reduced following the decoupling from the STN during the stimulation period (66% reduction in the population GP–GPi BUA coherence, $p<0.001$, Wilcoxon paired signed rank test) (Fig. 5A). The mean coherogram of GPi–GPi BUA pairs indicated that the decorrelation process of the BG output took place immediately (<1 s) after the stimulation initiation (Fig. 5B). A similar reduction occurred in the coherence between other GPi signals (Fig. 5C). Two exceptions to this reduction were the SU–SU coherence which was large in magnitude but not significant in its rank test due to the limited number of oscillating neurons, and the LFP–LFP coherence which was not reduced at all, since the LFPs are global signals with intrinsically high coherence between electrodes which are spaced closely.

Discussion

Our earlier studies have focused on the stimulation derived rate and pattern changes at the single neuron level (Bar-Gad et al., 2004; Erez et al., 2009; Moran et al., 2011). In this study we analyzed the oscillatory activity at the single neuron and population levels. Neuronal activity in the basal ganglia of the MPTP treated primates was characterized by oscillatory activity in the 10–15 Hz band of all the recorded signals. These signals are classically characterized as representing both the input (LFP) (Logothetis, 2003; Mitzdorf, 1985) and the output (SU and BUA) of the nuclei. Neuronal oscillations were evident in only a fraction of the neurons (SU) but were more abundant in the cumulative activity of multiple units (BUA). The oscillations were coherent both within each nucleus and between different nuclei prior to stimulation. STN-HFS reduced oscillations in both GP segments while the STN retained its oscillatory activity. However, the STN was functionally dissociated from its targets as evidenced by the drop in its coherence with its pallidal targets. This STN–GP dissociation in turn removed the coherence within the GPi, resulting in independent firing of the BG output neurons. The stimulation parameters used in this study were similar to those previously applied successfully in humans (Kuhn et al., 2008) and other animal studies trying to replicate the clinical environment (Hashimoto et al., 2003). However, in this study we have no direct measures of the clinical change in the parkinsonian symptoms and therefore we make no claims regarding the therapeutic value of the stimulation. The circular mono-polar contact of our macroelectrode is different from the multi-contact, typically bi-polar, electrode used clinically for DBS. This may lead to differences in the shape of the resulting electrical field (Butson and McIntyre, 2006; Carlson et al., 2010). The stimulation, however, had multiple common properties: the electrode impedance, the pulse waveform, amplitude and frequency. Thus, we believe that for the most part the effect of our stimulation resembles the one achieved by commercial DBS electrodes.

Neuronal oscillatory spiking activity can be assessed by looking at single neuron (SU) or small multi-neuron populations (BUA) (Moran and Bar-Gad, 2010). In line with previous studies (Schneidman et al., 2006), multi-neuron activity, which sums up the activity of 10–100 neurons, displayed more widespread and robust oscillations. BUA and SU measures displayed the same basic properties in the parkinsonian state and the same oscillation reduction during stimulation. However, the BUA, which more reliably represents the population, displayed these properties to a larger extent and was thus used to quantify the observed phenomena. The LFP coherence within and between nuclei was the least affected by the stimulation. This may be influenced by two factors: (a) Low frequency signals (such as LFP) spread passively over larger distances within the brain resulting in low spatial resolution of the signal and consequently high coherence. (b) The LFP signal is a result of multiple processes, primarily post synaptic potentials which represent the input to the specific brain area. Thus, an additional oscillatory

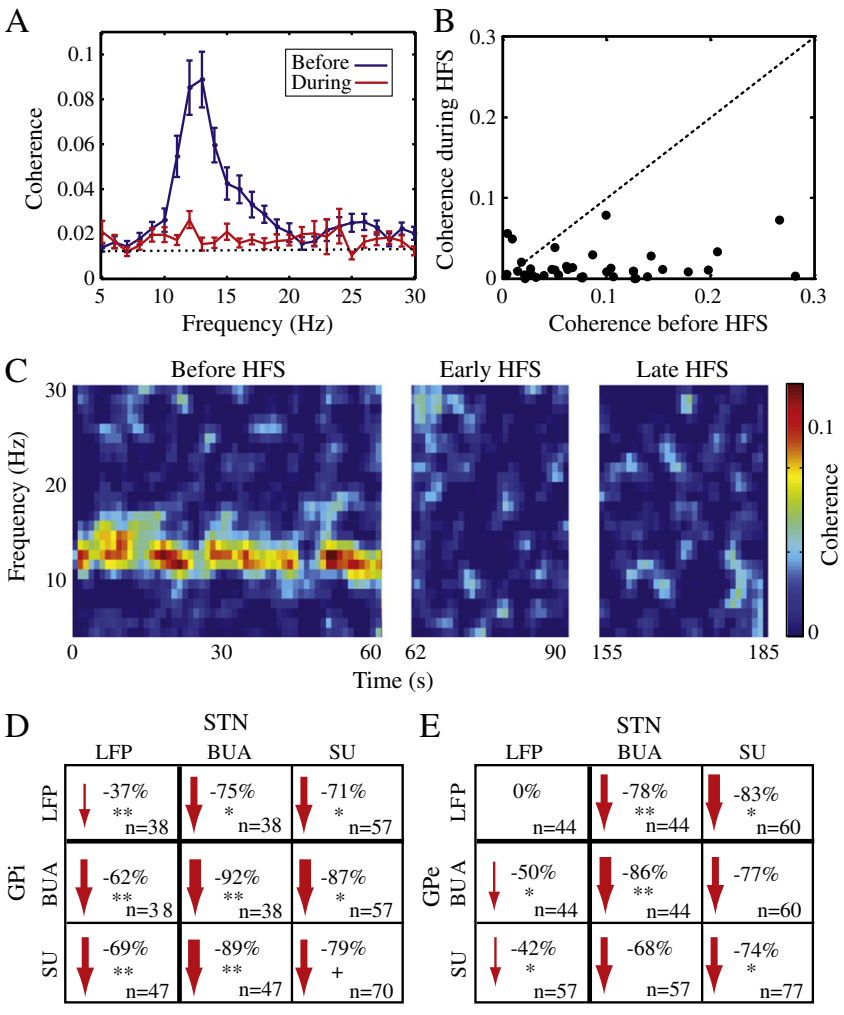

Fig. 3. Coherence between the STN and its targets. (A) Mean coherence of the STN-BUA and GPi-BUA (n = 38) before (blue) and during (red) STN-HFS. The dotted line denotes the baseline coherence level. (B) Scatter plot of the single pairs of STN-BUA to GPi-BUA peak coherence values before vs. during stimulation. The diagonal dotted line marks no changes in the coherence. Pairs appearing below the diagonal line mark a reduction in the coherence during the stimulation. (C) Mean coherogram over all STN-BUA and GPi-BUA pairs demonstrating the temporal evolution of the coherence. (D-E) Stimulation induced changes in the coherence of the STN with its targets, (D) the GPi and (E) the GPe. The table presents changes in the coherence between different signals: LFP, BUA and SU. Each cell contains the number of pairs, the mean change in the peak coherence value and the significance of the change over all the pairs (Wilcoxon paired signed rank test, ** $p<0.001$, * $p<0.01$, + $p<0.05$). The arrow thickness denotes the magnitude of the change in the coherence.

input such as from the cortex or striatum may lead to coherent activity of their targets the STN and GPi (Moran and Bar-Gad, 2010).

Although many of the neurons in the STN underwent complete inhibition (Moran et al., 2011), some of the non-inhibited neurons maintained their oscillatory activity resulting in no reduction in STN-SU oscillations. The BUA, which sums the activity of both inhibited and non-inhibited neurons, displayed a significant oscillation reduction which is consistent with previous neuronal population studies (Meissner et al., 2005). This is also in line with the stimulation induced reduction in STN oscillations which occurred in parallel with the improvement in motor performance (Kuhn et al., 2008). The reduction of spiking oscillations in both pallidal segments concurs with previous observations of reduced pallidal LFP oscillations (Brown et al., 2004). The larger fraction of oscillating neurons and increased magnitude of oscillations in the GPi relative to the GPe are also in agreement with previous studies (Heimer et al., 2002).

Simultaneous recording in STN and its targets revealed that while the somas of STN neurons were primarily inhibited by the stimulation, the axons were activated by the stimulation as evidenced by the locking of GP neuronal activity to the stimulation pulses (Hashimoto et al., 2003; Moran et al., 2011). This resulted in a decoupling of the stimulated nucleus (STN) from its target (GPi). This is further evidenced by the decrease in coherence between the STN and the GPi despite the persistence of some oscillatory activity in the STN. A study revealing the reduction of STN–GPi LFP coherence in PD patients following dopaminergic treatment (Brown et al., 2001) hints that such decoupling is tightly related to a reduction in PD symptoms. The reduction of the GPe–GPi coherence that we observed may further contribute to the decoupling of the GPi from the sources of its input. Our current measures cannot separate the direct effect on this coherent activity derived from direct activation from the GPe and the effect mediated through the STN. However, the dramatically larger reduction of the STN–GPi coherence relative to the GPe–GPi coherence hints that the STN is the primary source of change during the stimulation.

Neuronal firing in the GPi of the normal animal is characterized by "randomness" in both time (Poissonian spike distribution) and space (uncorrelated activity) (Heimer et al., 2002; Nini et al., 1995; Raz et al., 2000). These two properties lead to a baseline state of tonic inhibition of their thalamic targets as a result of the minimal fluctuations of the sum of inhibitory inputs received by a thalamic neuron. In PD, neuronal firing becomes correlated in time due to oscillations, and in space

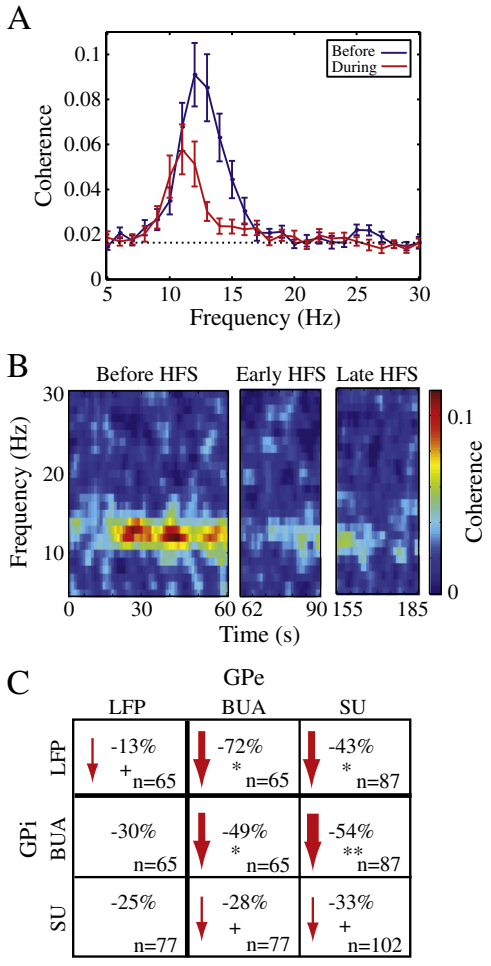

Fig. 4. Coherence between the GPe and the GPi. (A) Mean coherence of the GPe-BUA and GPi-BUA (n = 65) before (blue) and during (red) STN-HFS. The dotted line denotes the baseline coherence level. (B) Mean coherogram over all GPe-BUA and GPi-BUA pairs demonstrating the temporal evolution of the coherence. (C) Stimulation induced changes in the coherence of the GPe with the GPi. The table presents changes in the coherence between different signals: LFP, BUA and SU. Each cell contains the number of pairs, the mean change in the peak coherence value and the significance of the change over all the pairs (Wilcoxon paired signed rank test, ** $p<0.001$, * $p<0.01$, + $p<0.05$). The arrow thickness denotes the magnitude of the change in the coherence.

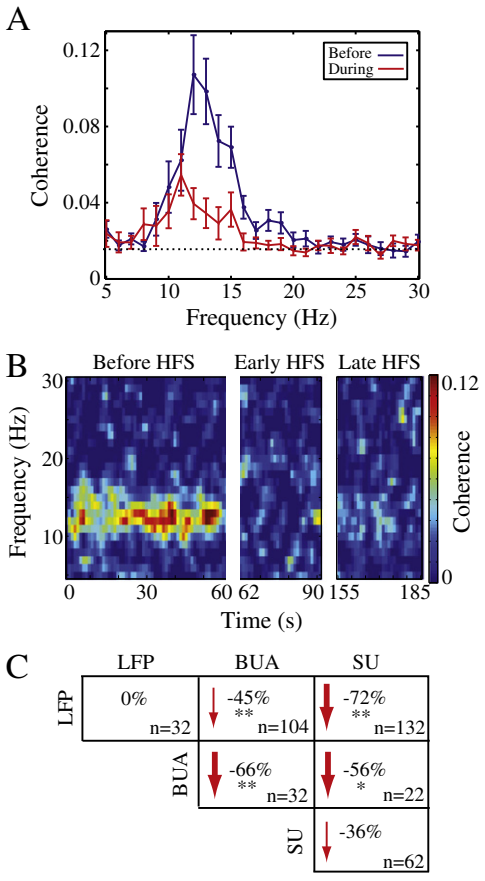

Fig. 5. Coherence within the GPi. (A) Mean coherence between the BUA on different electrodes in the GPi (n = 32) before (blue) and during (red) STN-HFS. The dotted line denotes the baseline coherence level. (B) Mean coherogram demonstrating the temporal evolution in the BUA coherence within the GPi. (C) Stimulation induced changes in the coherence of different signals within the GPi. Each cell contains the number of pairs, the mean change in the peak coherence value and the significance of the change over all the pairs (Wilcoxon paired signed rank test, ** $p<0.001$, * $p<0.01$). The arrow thickness denotes the magnitude of the change in the coherence.

resulting in increased coherence (Heimer et al., 2002; Nini et al., 1995; Raz et al., 2000). This, in turn, is hypothesized to lead to major temporal fluctuations in the sum of the inhibitory GPi output. Our results demonstrate that STN-HFS reduces both types of correlations resulting in the "randomization" of BG output. The stimulation introduces new temporal correlations due to spike locking to the stimulation pulses (Hashimoto et al., 2003; Moran et al., 2011). However, this short latency (8 ms) regularization does not alter the irregularity on larger time scales of tens to hundreds of milliseconds, and may not lead to major alterations in thalamic excitability because of the long integration time of the inhibitory post synaptic potentials (Yamamoto et al., 1984). The STN currently serves as the primary target for stimulation in PD, however, GPi stimulation has demonstrated large clinical benefits as well (Rodriguez-Oroz et al., 2005). The observed changes in the temporal structure of GPi output to the thalamus in this study may potentially play the same role in the amelioration of PD symptoms through GPi DBS as pallidal output undergoes grossly the same changes (Bar-Gad et al., 2004; McCairn and Turner, 2009). Finally, it is important to note that our results describe the baseline activity of the pathological basal ganglia during rest and the changes occurring in this state during DBS. Further work is needed to shed light on the effect of DBS on the encoding of the animal behavior (e.g. movement).

A computational model of the cortico-BG loop reveals a failure in information transmission by thalamic neurons during parkinsonism that was attributed to coherent thalamic modulation by BG output (Guo et al., 2008; Rubin and Terman, 2004). In accordance with this model, our results show coherent oscillatory BG output which could potentially lead to large variations in thalamic activity due to the fluctuating inhibitory drive (Fig. 6A). STN-HFS led to a reduction in the oscillatory synchrony of GPi and the return to independent activity. These reduced temporal fluctuations in the sum of the inhibitory input to the thalamus potentially enable high fidelity transmission of information to the cortex (Fig. 6B). Our results are congruent with theoretical work (Cagnan et al., 2009; Guo et al., 2008; Rubin and Terman, 2004) suggesting that the level of correlated oscillatory activity, rather than the baseline firing rate of the GPi and its modulation by HFS, is a major pathophysiological factor involved in the manifestation of PD clinical symptoms.

The findings of this study show for the first time changes in coherence in the neuronal spiking activity within and between different nuclei of the BG during STN-HFS. These results highlight that the major change occurring during STN-HFS in parkinsonian primates is the decoupling of the STN from the GPi, leading to a reduction in coherent BG output.

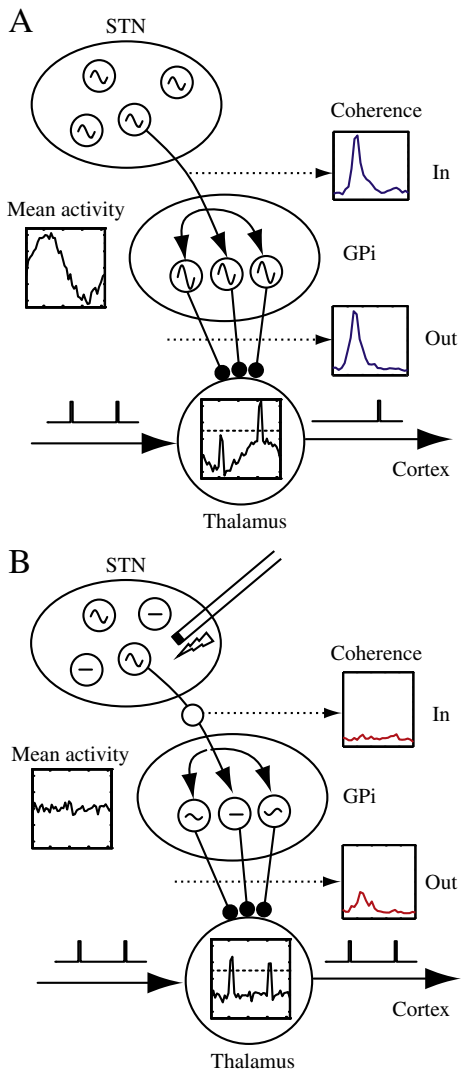

Fig. 6. Changes in BG control during STN-HFS. (A) In the parkinsonian state, prior to stimulation, coherent oscillations in the GPi driven by the oscillatory input from STN lead to large fluctuations in the inhibitory output of the BG. The thalamus sums the input to be transmitted to the cortex from other sources with the revered inhibitory GPi activity. The induced variation of thalamic activity leads to abnormal transmission of information to the cortex as only some of the inputs cross the threshold required to activate the thalamic neuron (dotted line in the thalamus box). (B) During stimulation, the STN's oscillatory output is decoupled from the GPi (depicted as a circle on the output arrow leaving the STN). This leads to a reduction in GPi neuronal oscillations and to reduced coherence among these neurons. The sum of GPi output becomes random in space and time leading to a constant level of inhibition of the thalamus, enabling the reliable transmission of information to the cortex. The experimental results of incoming coherence (STN–GPi BUA) and the output coherence (BUA within GPi) are plotted before (A—blue) and during (B—red) stimulation.

This stimulation induced decorrelation may form the basis for the therapeutic mechanism behind DBS in PD.

Funding

This study was supported by Israel Science Foundation (ISF) grant (1000-05); Legacy Heritage Biomedical Program of the ISF grant (981-10) and Ministry of Health (MOH) grant (3-4033).

Acknowledgments

We thank M. Dror, K. McCairn for animal care, A. Tzameret for recording assistance and K. Belelovsky for technical help.

References

Adler, A., Joshua, M., Rivlin-Etzion, M., Mitelman, R., Marmor, O., Prut, Y., Bergman, H., 2010. Neurons in both pallidal segments change their firing properties similarly prior to closure of the eyes. J. Neurophysiol. 103, 346–359.
Albin, R.L., Young, A.B., Penney, J.B., 1989. The functional anatomy of basal ganglia disorders. Trends Neurosci. 12, 366–375.
Bar-Gad, I., Elias, S., Vaadia, E., Bergman, H., 2004. Complex locking rather than complete cessation of neuronal activity in the globus pallidus of a 1-methyl-4-phenyl-1,2,3,6-tetrahydropyridine-treated primate in response to pallidal microstimulation. J. Neurosci. 24, 9410–9419.
Benazzouz, A., Gross, C., Feger, J., Boraud, T., Bioulac, B., 1993. Reversal of rigidity and improvement in motor performance by subthalamic high-frequency stimulation in MPTP-treated monkeys. Eur. J. Neurosci. 5, 382–389.
Bergman, H., Wichmann, T., DeLong, M.R., 1990. Reversal of experimental parkinsonism by lesions of the subthalamic nucleus. Science 249, 1436–1438.
Bergman, H., Wichmann, T., Karmon, B., DeLong, M.R., 1994. The primate subthalamic nucleus. II. Neuronal activity in the MPTP model of parkinsonism. J. Neurophysiol. 72, 507–520.
Brown, P., Oliviero, A., Mazzone, P., Insola, A., Tonali, P., Di Lazzaro, V., 2001. Dopamine dependency of oscillations between subthalamic nucleus and pallidum in Parkinson's disease. J. Neurosci. 21, 1033–1038.
Brown, P., Mazzone, P., Oliviero, A., Altibrandi, M.G., Pilato, F., Tonali, P.A., Di Lazzaro, V., 2004. Effects of stimulation of the subthalamic area on oscillatory pallidal activity in Parkinson's disease. Exp. Neurol. 188, 480–490.
Butson, C.R., McIntyre, C.C., 2006. Role of electrode design on the volume of tissue activated during deep brain stimulation. J. Neural. Eng. 3, 1–8.
Cagnan, H., Meijer, H.G., van Gils, S.A., Krupa, M., Heida, T., Rudolph, M., Wadman, W.J., Martens, H.C., 2009. Frequency-selectivity of a thalamocortical relay neuron during Parkinson's disease and deep brain stimulation: a computational study. Eur. J. Neurosci. 30, 1306–1317.
Carlson, J.D., Cleary, D.R., Cetas, J.S., Heinricher, M.M., Burchiel, K.D., 2010. Deep Brain Stimulation (DBS) Does Not Silence Neurons in Subthalamic Nucleus in Parkinson's Patients. J. Neurophysiol. 103, 962–967.
DeLong, M.R., 1990. Primate models of movement disorders of basal ganglia origin. Trends Neurosci. 13, 281–285.
Erez, Y., Czitron, H., McCairn, K., Belelovsky, K., Bar-Gad, I., 2009. Short-term depression of synaptic transmission during stimulation in the globus pallidus of 1-methyl-4-phenyl-1,2,3,6-tetrahydropyridine-treated primates. J. Neurosci. 29, 7797–7802.
Erez, Y., Tischler, H., Moran, A., Bar-Gad, I., 2010. Generalized framework for stimulus artifact removal. J. Neurosci. Methods 191, 45–59.
Filali, M., Hutchison, W.D., Palter, V.N., Lozano, A.M., Dostrovsky, J.O., 2004. Stimulation-induced inhibition of neuronal firing in human subthalamic nucleus. Exp. Brain Res. 156, 274–281.
Fox, S.H., Brotchie, J.M., 2010. The MPTP-lesioned non-human primate models of Parkinson's disease. Past, present, and future. Prog. Brain Res. 184, 133–157.
Guo, Y., Rubin, J.E., McIntyre, C.C., Vitek, J.L., Terman, D., 2008. Thalamocortical relay fidelity varies across subthalamic nucleus deep brain stimulation protocols in a data-driven computational model. J. Neurophysiol. 99, 1477–1492.
Hashimoto, T., Elder, C.M., Okun, M.S., Patrick, S.K., Vitek, J.L., 2003. Stimulation of the subthalamic nucleus changes the firing pattern of pallidal neurons. J. Neurosci. 23, 1916–1923.
Heimer, G., Bar-Gad, I., Goldberg, J.A., Bergman, H., 2002. Dopamine replacement therapy reverses abnormal synchronization of pallidal neurons in the 1-methyl-4-phenyl-1,2,3,6-tetrahydropyridine primate model of parkinsonism. J. Neurosci. 22, 7850–7855.
Kuhn, A.A., Kempf, F., Brucke, C., Gaynor, D.L., Martinez-Torres, I., Pogosyan, A., Trottenberg, T., Kupsch, A., Schneider, G.H., Hariz, M.I., Vandenberghe, W., Nuttin, B., Brown, P., 2008. High-frequency stimulation of the subthalamic nucleus suppresses oscillatory beta activity in patients with Parkinson's disease in parallel with improvement in motor performance. J. Neurosci. 28, 6165–6173.
Levy, R., Ashby, P., Hutchison, W.D., Lang, A.E., Lozano, A.M., Dostrovsky, J.O., 2002. Dependence of subthalamic nucleus oscillations on movement and dopamine in Parkinson's disease. Brain 125, 1196–1209.
Limousin, P., Pollak, P., Benazzouz, A., Hoffmann, D., Le Bas, J.F., Broussolle, E., Perret, J.E., Benabid, A.L., 1995. Effect of parkinsonian signs and symptoms of bilateral subthalamic nucleus stimulation. Lancet 345, 91–95.
Logothetis, N.K., 2003. The underpinnings of the BOLD functional magnetic resonance imaging signal. J. Neurosci. 23, 3963–3971.
McCairn, K.W., Turner, R.S., 2009. Deep brain stimulation of the globus pallidus internus in the parkinsonian primate: local entrainment and suppression of low-frequency oscillations. J. Neurophysiol. 101, 1941–1960.
Meissner, W., Leblois, A., Hansel, D., Bioulac, B., Gross, C.E., Benazzouz, A., Boraud, T., 2005. Subthalamic high frequency stimulation resets subthalamic firing and reduces abnormal oscillations. Brain 128, 2372–2382.
Mitzdorf, U., 1985. Current source-density method and application in cat cerebral cortex: investigation of evoked potentials and EEG phenomena. Physiol. Rev. 65, 37–100.
Moran, A., Bar-Gad, I., 2010. Revealing neuronal functional organization through the relation between multi-scale oscillatory extracellular signals. J. Neurosci. Methods 186, 116–129.
Moran, A., Bergman, H., Israel, Z., Bar-Gad, I., 2008. Subthalamic nucleus functional organization revealed by parkinsonian neuronal oscillations and synchrony. Brain 131, 3395–3409.
Moran, A., Stein, E., Tischler, H., Belelovsky, K., Bar-Gad, I., 2011. Dynamic stereotypic responses of Basal Ganglia neurons to subthalamic nucleus high-frequency stimulation in the parkinsonian primate. Front. Syst. Neurosci. 5, 21.

Nini, A., Feingold, A., Slovin, H., Bergman, H., 1995. Neurons in the globus pallidus do not show correlated activity in the normal monkey, but phase-locked oscillations appear in the MPTP model of parkinsonism. J. Neurophysiol. 74, 1800–1805.

Pogosyan, A., Yoshida, F., Chen, C.C., Martinez-Torres, I., Foltynie, T., Limousin, P., Zrinzo, L., Hariz, M.I., Brown, P., 2010. Parkinsonian impairment correlates with spatially extensive subthalamic oscillatory synchronization. Neuroscience 171, 245–257.

Raz, A., Vaadia, E., Bergman, H., 2000. Firing patterns and correlations of spontaneous discharge of pallidal neurons in the normal and the tremulous 1-methyl-4-phenyl-1,2,3,6-tetrahydropyridine vervet model of parkinsonism. J. Neurosci. 20, 8559–8571.

Rodriguez-Oroz, M.C., et al., 2005. Bilateral deep brain stimulation in Parkinson's disease: a multicentre study with 4 years follow-up. Brain 128, 2240–2249.

Rubin, J.E., Terman, D., 2004. High frequency stimulation of the subthalamic nucleus eliminates pathological thalamic rhythmicity in a computational model. J. Comput. Neurosci. 16, 211–235.

Schneider, J.S., Gonczi, H., Decamp, E., 2003. Development of levodopa-induced dyskinesias in parkinsonian monkeys may depend upon rate of symptom onset and/or duration of symptoms. Brain Res. 990, 38–44.

Schneidman, E., Berry, M.J., Segev, R., Bialek, W., 2006. Weak pairwise correlations imply strongly correlated network states in a neural population. Nature 440, 1007–1012.

Szabo, J., Cowan, W.M., 1984. A stereotaxic atlas of the brain of the cynomolgus monkey (*Macaca fascicularis*). J. Comp. Neurol. 222, 265–300.

Welter, M.L., Houeto, J.L., Bonnet, A.M., Bejjani, P.B., Mesnage, V., Dormont, D., Navarro, S., Cornu, P., Agid, Y., Pidoux, B., 2004. Effects of high-frequency stimulation on subthalamic neuronal activity in parkinsonian patients. Arch. Neurol. 61, 89–96.

Yamamoto, T., Noda, T., Miyata, M., Nishimura, Y., 1984. Electrophysiological and morphological studies on thalamic neurons receiving entopeduncuIo- and cerebellothalamic projections in the cat. Brain Res. 301, 231–242.

Zaidel, A., Arkadir, D., Israel, Z., Bergman, H., 2009. Akineto-rigid vs. tremor syndromes in Parkinsonism. Curr. Opin. Neurol. 22, 387–393.